Three-Dimensional Printing of Innovative Intramedullary Pin Profiles with Direct Metal Laser Sintering

Rupinder Singh ⓘ, Jashanpreet Singh Sidhu, Rishab, B.S. Pabla, and Ashwani Kumar

In the past one decade, use of intramedullary (IM) pins (Steinmann pins or end-threaded pins) as implants for the repair of long bone fractures in canine has been widely reported. One of the major limitations of these pins is implant dislodgement and proximal migration mainly due to less retention rate in the proximal end. Some studies have reported the fabrication of IM pins for canine by conventional machining methods, but hitherto little has been reported on the innovative profiles of IM pins for canine prepared by direct metal laser sintering (DMLS) of 17-4 precipitation-hardening (PH) stainless steel (SS). This paper reports the fabrication and process parametric optimization for innovative IM pin profiles on 17-4PH SS with DMLS. The selected output parameters are surface hardness (HV), surface roughness (Ra), and dimensional error (Δd). The results of the study suggest that laser power 100 W, scan speed 1200 mm/s, and layer thickness-0.04-mm are the best settings of DMLS from a multi-factor optimization viewpoint. The results have been supported with scanning electron microscopy-based photo-micrographs, 3D rendered images, porosity (%), and grain size number.

1. Introduction

In the recent past, additive manufacturing (AM) processes have been widely explored for bio-medical applications (Ref 1). In almost all AM processes, functional parts are prepared from computer-aided design (CAD) models, usually by the following layer by layer deposition techniques (Ref 1-2). In AM, desired geometrical accuracy is obtained by producing minimal possible waste. These processes can manufacture complex geometrical components, especially for biomedical applications. Along with biomedical applications, AM processes are being extensively used in the aerospace, automotive, defence, and construction industry (Ref 3-4). As per reported literature, the AM has been extensively used for printing biomedical models, biomaterials, dentistry, and orthopedic scaffolds and implants (Ref 5). The customized/patient-specific product is being designed and fabricated by AM techniques more efficiently. Additively manufactured cranioplasty implants have accuracy that meets the current best practice (Ref 6). It saves time and cost by creating an ideal fit implant (Ref 7). The success of any medical device depends on the choice of proper

material to fulfil the expected function (Ref 8). The performance of biomedical material is dependent on two factors: bio functionality and biocompatibility (Ref 9). Biofunctionality deals with the ability of the equipment to perform the required function, whereas biocompatibility refers to the compatibility of the material in the body. The number of metals and alloys that are used for medical implants is limited because of their biocompatibility-related issues. The SS316L, Ti alloys, and Co-Cr alloys are the mainly used metals for angioplasty, fracture fixation, and bone remodeling. These alloys provide long-term stability under highly reactive in-vivo conditions and have excellent mechanical properties (Ref 10). The Ti alloys are the most significantly used metallic materials in orthopedic and dental implants because of their corrosion resistance, biocompatibility, and excellent mechanical properties (Ref 11). The SS316L an alloy of Fe, Ni, and Cr is also widely used in medical applications (Ref 12). It has been reported that inadequate wear resistance is a major drawback of Ti alloys. Mini screw implants made of SS and Ti alloys give similar mechanical stability and histologic response. These both fit for clinical uses of immediate orthodontic loading (Ref 13). According to in vitro cytotoxicity results, 17-4 PH SS foams show sufficient biocompatibility. It can be considered that 17-4 PH SS is a potential material for biomedical applications (Ref 14).

The DMLS is one of the recent AM technologies for rapid manufacturing (Ref 15). In DMLS, the laser is used as the power source to sinter material layer-by-layer. It is favorable for complex and dense geometric components (Ref 16). It does not melt the powder, so less energy is required. Pure metals or metal alloys are used for fabricating the components. Even mixtures of different metal powders can also be successfully printed. It has been reported that reduction in process time and cost optimization of process parameters is very important in DMLS (Ref 17). Some studies have reported that in the DMLS process, hardness is most affected by hatch distance (Ref 18), and build direction has a significant effect on Ra and Δd (Ref 19).

Rupinder Singh, Jashanpreet Singh Sidhu, and **B.S. Pabla**, Department of Mechanical Engineering, National Institute of Technical Teachers Training and Research, Chandigarh, India; **Rishab**, Department of Mechanical Engineering, National Institute of Technical Teachers Training and Research, Chandigarh, India; and Department of Mechanical Engineering, Punjab Engineering College, Chandigarh, India; and **Ashwani Kumar**, Department of Veterinary Surgery and Radiology, Guru Angad Dev Veterinary and Animal Science University, Ludhiana, Punjab, India. Contact e-mail: rupindersingh@nitttrchd.ac.in.
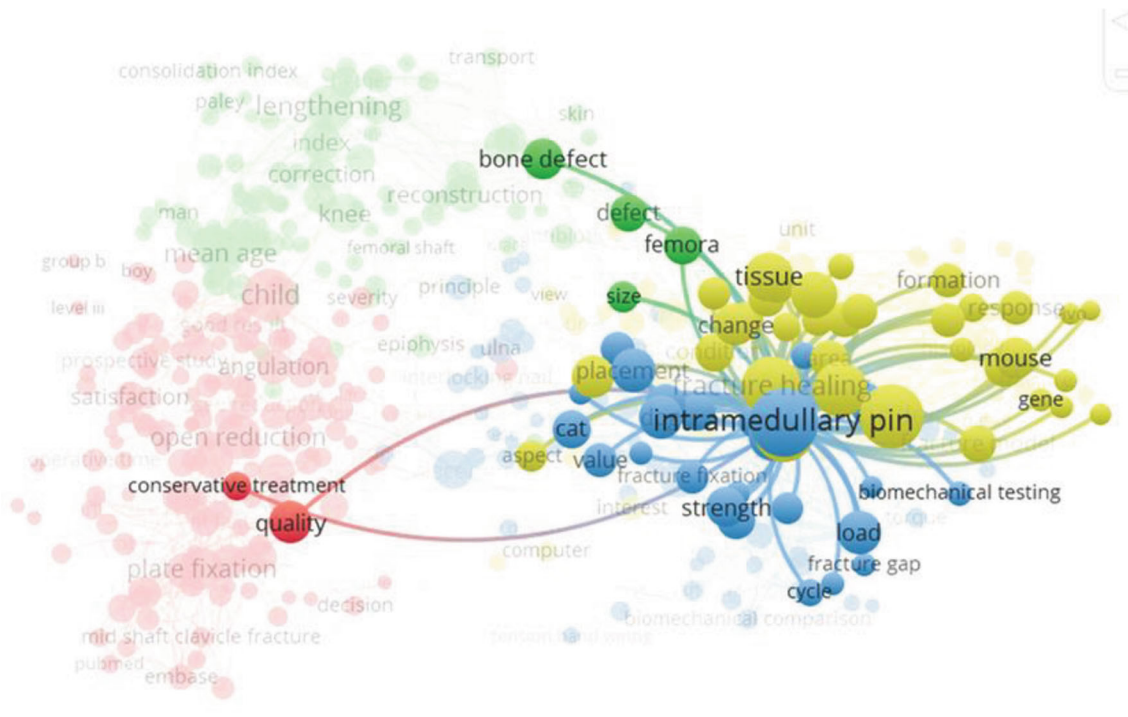
Nowadays due to excessive vehicular congestion, there are high occurrences of long bone fractures in dogs (Ref 20). Comminute, oblique, or multiple fractures (classified as fractures or unstable configuration) occurring due to vehicular trauma or fall from height is very common now a days. For such cases in orthopedic surgery, IM nailing is a standard procedure (in long bone fractures) (Ref 21). IM pinning is a commonly used technique for such veterinary patients. In this technique, the IM pin is passed through the intramedullary cavity of the bone for repairing the fractures. Usually, a simple IM pin is not suggested to treat long bone fractures in dogs especially of unstable configuration as it does not counteract compression and rotational forces. Simple IM pins cannot be used alone because they may not provide adequate traction and rotational stability (Ref 22). Fractures of unstable configuration

are treated by static or rigid fixation techniques such as bone plating and intramedullary interlocking nailing but they defy the principle of biological osteosynthesis. The concept of biological osteosynthesis emphasis that fracture fixation should be attempted in a minimally invasive fashion, and soft tissue structures should be preserved around the site of fracture. Osteosynthesis is a complex process for canine long bones as it requires knowledge of biomechanical principles, biology, and surgical techniques (Ref 23). It has been reported that fractures treated with bone plates have a higher success rate (91%) as compared to IM pinning (64.2%) (Ref 24). On the other hand, IM pins provide less soft tissue dissection than bone plating (Ref 25). Less rigid fixation techniques like IM pinning, bridging plate helps in healing faster than fractures repaired with rigid fixation techniques such as bone plating (Ref 26). In the fixation of mandibular condyle fractures, Ti-based IM implants give more strength and stiffness than mini plates (Ref 27). The end threaded pin is a modification of a simple Steinmann pin. The threaded portion in end threaded pin provides better holding of the pin in the distal end of the bone (Ref 28). Fig. 1 shows fracture repaired by end threaded pin. An IM fully threaded pin provides good rotational stability in both proximal and distal ends (Ref 29). End threaded pin can be modified by using more threads and of different profiles. Positive profile threads can be used in the proximal end of the bone to provide better holding of threaded pins. It may increase the retention rate in the proximal end of the bone.

For ascertaining the research gap, the web of science database (for years 1999–2021) has been explored by putting the keyword 'intramedullary pins', and 860 results were obtained from the core collection. These results were further sorted out based upon the highest number of citations, and the top 500 articles were selected. After this, another keyword

Fig. 1. Fracture repaired with end threaded pin (in mix breed dog)

Fig. 2. Bibliographic analysis for keyword 'intramedullary pins'

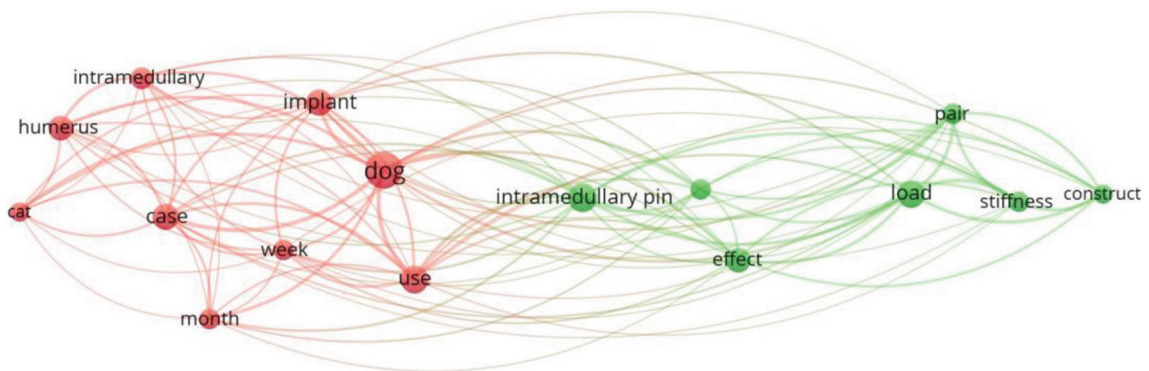**Fig. 3.** Research gap analysis for keyword 'intramedullary pins'

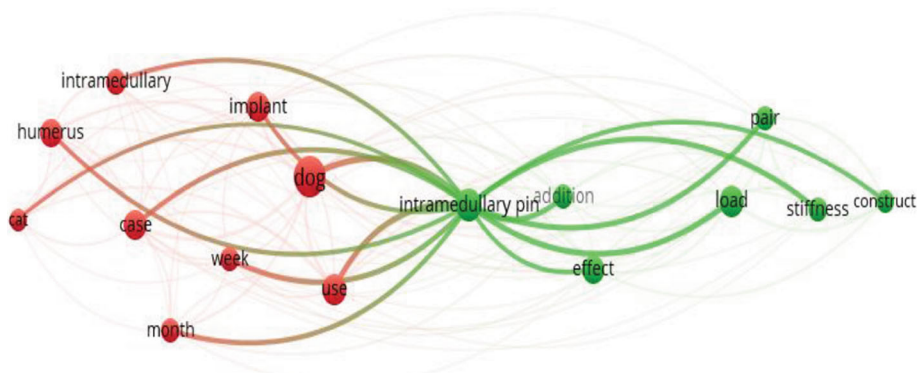**Fig. 4.** Bibliographic analysis for keyword 'intramedullary pins for canine'

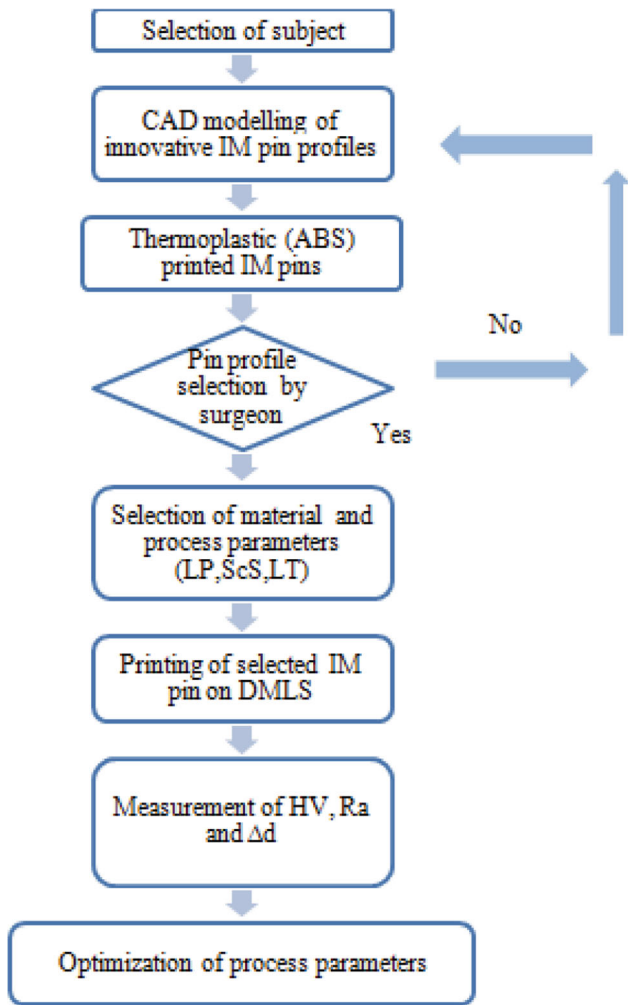**Fig. 5.** Research gap analysis for the keyword 'intramedullary pins for canine'

Fig. 6. Process flow diagram for the present study

'intramedullary pins for canine' was used, and 30 results were obtained. For analysis of these results, VOS viewer open source software has been used. By selecting a minimum number of occurrences of term '5', 710 terms met the threshold out of 11686 terms. Further for these 710 terms, relevance score was calculated, and the top 60% terms '426' were used for analysis. Based upon the calculated relevance score, Fig. 2 shows the networking diagram as bibliographic analysis. As observed from Fig. 2, 04 different clusters were noticed for previous studies. By selecting the intramedullary pin as nodal point, research gap analysis has been highlighted (Fig. 3). Similarly, Fig. 4 and 5, respectively, show bibliographic analysis for the keyword 'intramedullary pins for canine' and research gap analysis for the keyword 'intramedullary pins for canine'

The literature review reveals that IM pins as implants for the repair of long bone fractures in the canine have been widely used. One of the major limitations of these pins is implant dislodgement and proximal migration mainly due to less retention rate in the proximal end. Some studies have reported the fabrication of IM pins for canine by conventional machining methods, but hitherto little has been reported on the innovative profiles of IM pins for canine prepared by DMLS of 17-4 PH SS. This study reports the fabrication and process parametric optimization for innovative IM pin profiles on 17-4PH SS with DMLS.

2. Methodology

The present study was completed in 06 stages. Figure 6 shows the process flow diagram for the present study.

- Stage 1-Subject selection: The femur bone of the canine (pitbull of age 1 year) was selected.
- Stage 2-CAD modeling of innovative IM pin profiles: The CAD files of innovative profiles of IM pins were generated with Solidworks software for the selected bone part.
- Stage 3-Thermoplastic acrylonitrile butadiene styrene (ABS) printed IM pins: The innovative profiles IM pins were printed on a thermoplastic-based fused deposition modeling (FDM)-based printer by using ABS material.
- Stage 4-Pin profile selection by the surgeon: The best profile pin from these pins was selected by the surgeon based upon his experience.
- Stage 5-Selection of material and process parameters: The material selected was 17-4 PH SS and process parameters were LP, ScS, and LT.
- Stage 6-Printing of selected IM on DMLS: IM pin selected by the surgeon was fabricated on DMLS by using different process parameters.
- Stage 7-Measurement of HV, Ra, and Δd: Measurement of hardness was performed by using microhardness tester (in HV), Ra was measured by surface roughness tester (in μm), and Δd was measured by comparing the length of printed pins with the CAD file by using the digital vernier caliper.
- Stage 8-Optimization of process parameters: Optimization was performed from a multi-factor optimization viewpoint.

3. Experimentation

3.1 Printing the CAD File of Pins on FDM

For the femur bone of the canine (Fig. 7a) based upon the selected subject), innovative profiles on IM pins were designed (Fig. 7b, c, and d) in consultation with a veterinary surgeon. The CAD files of these innovative profile pins were generated using Solidworks. CAD files of innovative IM pins were converted into standard triangulation language (STL) format.
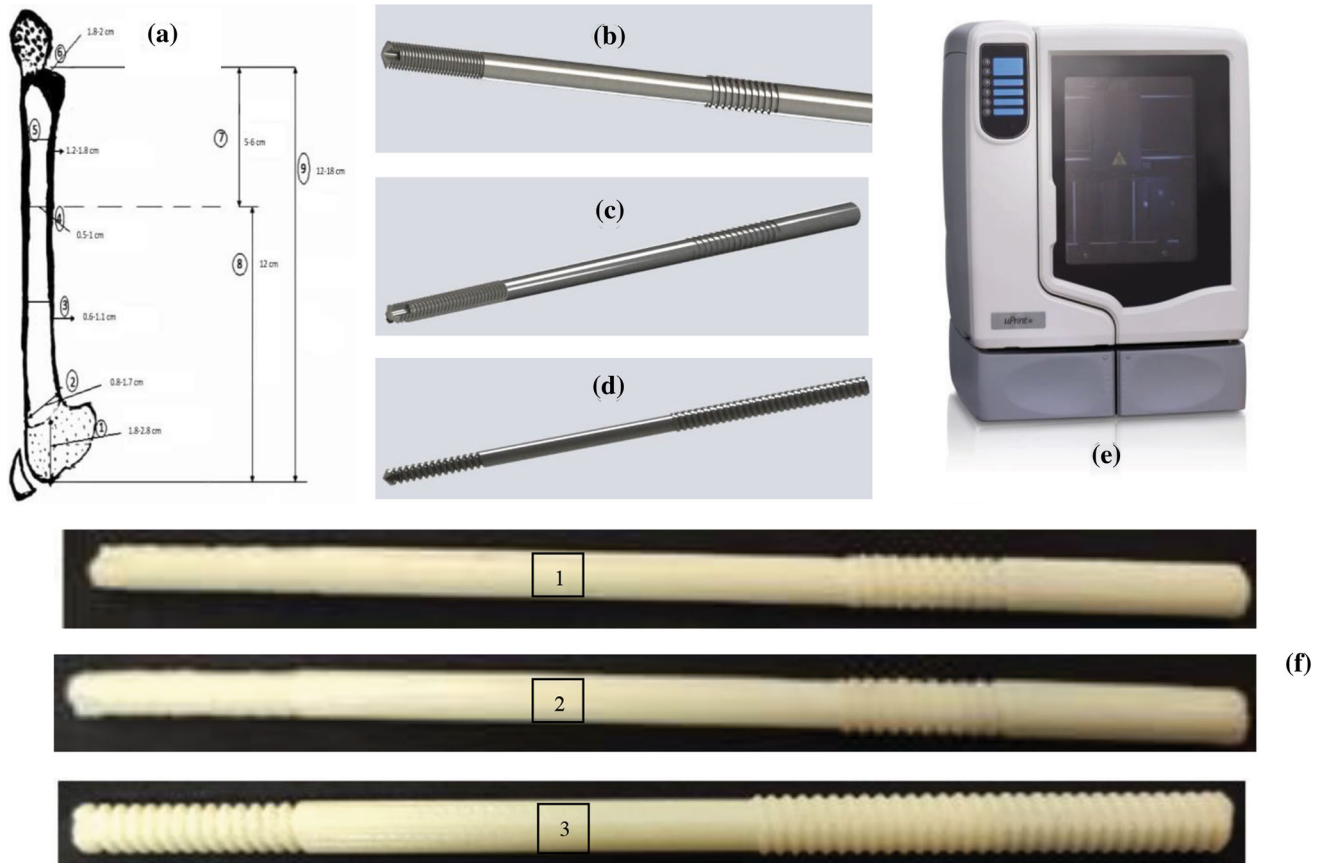
Fig. 7. (a) Selected bone for IM pins (b) CAD of simple threaded pin (c) CAD of tapered threaded pin (d) CAD file of the double-threaded pin (e) FDM printer (f) ABS printed threaded pin
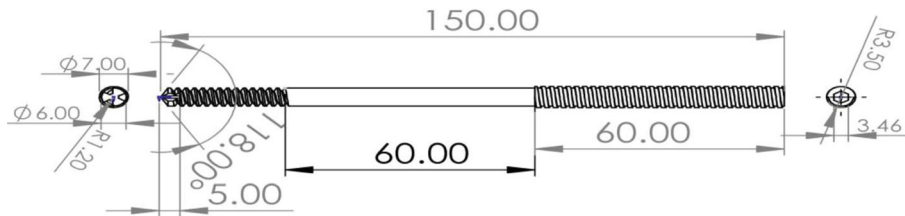

Fig. 8. Detailed drawing of selected IM pin

The files in STL format were imported in CatalystEX software, and slicing of CAD files was performed. After slicing the CAD file, the orientation and density of pins were selected. Different pin profiles were printed on a thermoplastic-based FDM printer (Fig. 7e). The commercial P430 (ABS model material) and P400-SR (soluble support material) provided by Stratasys, USA was used in this study. From the different pin profiles printed, Pin no 3 (double threaded IM pin) has been selected by the surgeon as shown in Fig. 7(f). The selected IM profile was used for further fabrication on DMLS.

It has been reported that the IM pin should have a diameter of 50-70% of the intramedullary cavity of the bone (Ref 30). In the present case study length of the pin = 150 mm. The tip was made taper to make drilling easier into the cancellous bone (Fig. 8). The other specifications are:

Pitch of V threads = 1.5 mm
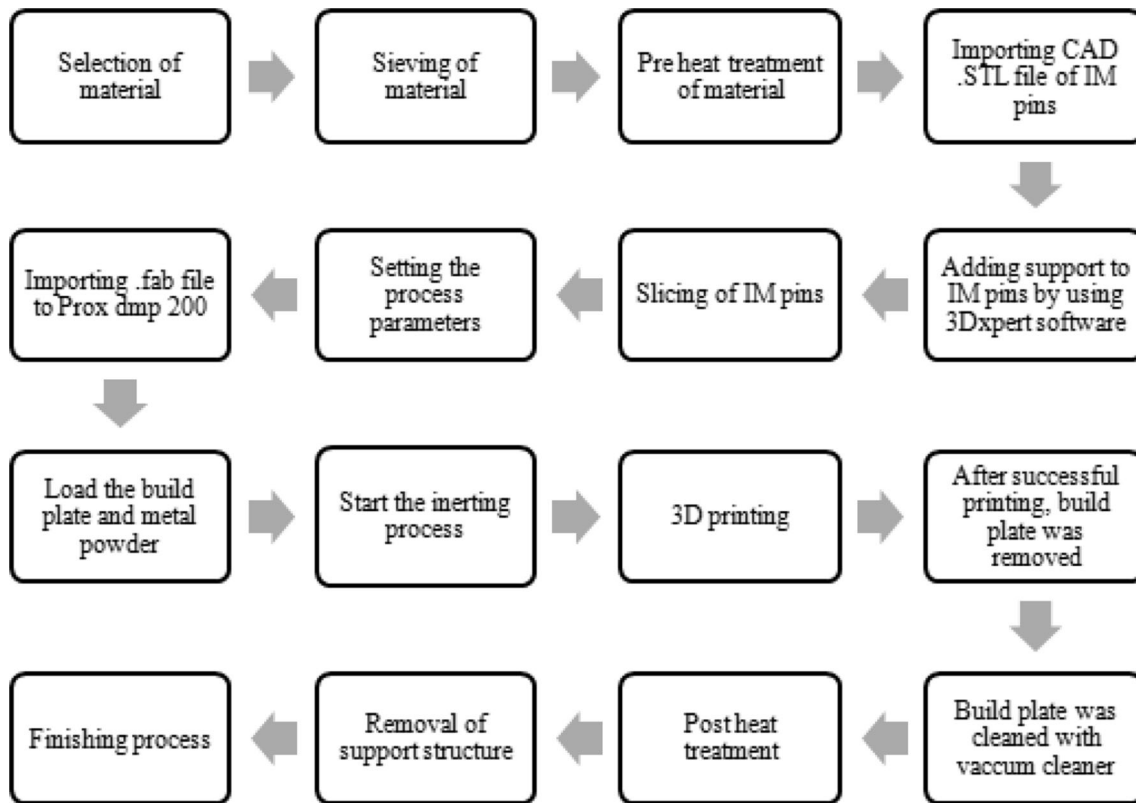
Fig. 9. Process flow for printing pins in DMLS

Pitch of square threads = 2 mm
Diameter of larger end = 7 mm
Diameter of the smaller end of pin= 6 mm

3.2 Fabrication of Pins on DMLS

In this case study, the material selected for printing IM pins was 17-4 PH SS. The metallic powder was preheated in the furnace for removing the moisture present. The CAD file in '.STL' format was imported in 3Dxpert software. Inclined wall support was provided to the pins for reducing the residual stresses. After adding support to the pins, the slicing of the CAD file was performed. Recalculating of slicing was done to change the process parameters (like LP, ScS, and LT). The process flow diagram for DMLS is shown in Fig. 9.

Based upon Fig. 9, 10 shows a diagrammatical representation for all steps. For printing of the IM pins, the design of the experiment (DOE) based upon Taguchi L9 orthogonal array (O.A) was followed (Table 1 and 2). After changing the process parameters, final slicing was carried out. The file was imported in Proxdmp 200 in .fab format. Build plate of material

Z8C17(steel) was loaded into the machine. Argon gas was used to provide an inert atmosphere in the machine chamber. Post-heat treatment was performed to remove residual stresses and to improve mechanical properties. Pins and support were removed from the build plate by using wire electrical discharge machining (WEDM).

4. Results and Discussion

After the printing of pins at different process parameters (as per Table 2); HV, Ra, and Δd were measured, and the corresponding signal to noise (SN) ratios were calculated using Minitab 17 software (Table 3). For SN calculations in the case of HV, it required to be maximum the better type case, so for this case, SN ratio can be calculated as:

$$\eta = -10 \log \left[\frac{1}{n} \sum_{k=1}^{n} \frac{1}{y^2} \right]$$
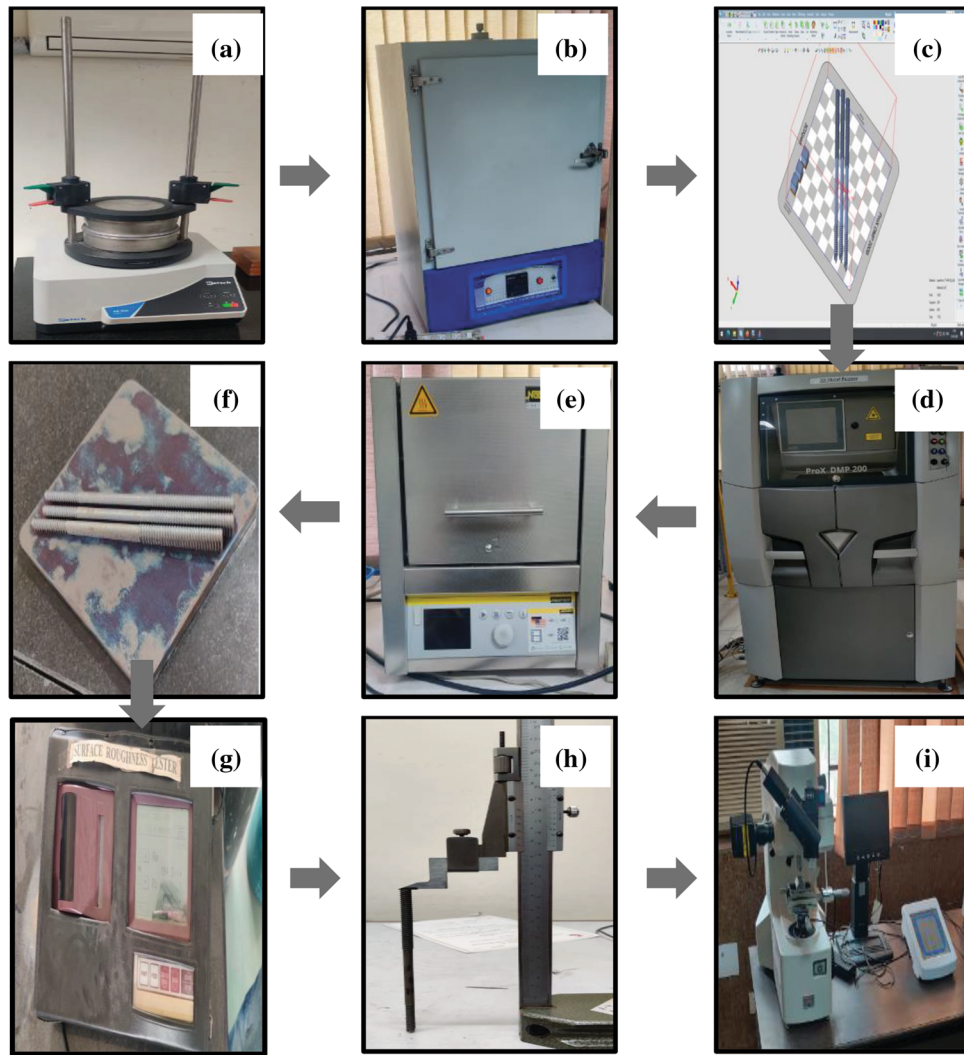
Fig. 10. (a) Sieving of powder, (b) Pre-heat treatment of powder, (c) Adding support to the pins in 3Dxpert software, (d) DMLS (proxdmp 200), (e) Post-heat treatment of IM pins, (f) Pins on build plate after post-heat treatment, (g) Surface roughness tester, (h)Vertical Vernier caliper, (i) Microhardness tester

Table 1. DMLS process parameters and their levels

Process parameter, s	A: LP, W	B: ScS, mm/s	C: LT, mm
Level 1	100	1000	0.02
Level 2	120	1200	0.03
Level 3	140	1400	0.04

For properties Ra and Δd smaller is better type case was selected and SN ratios can be calculated as;

$$\eta = -10 \log \left[\frac{1}{n} \sum_{k=1}^{n} y^2 \right]$$

Table 2. DOE for selected parameters

Exp. no.	LP, W	ScS, mm/s	LT, mm
1	100	1000	0.02
2	100	1200	0.03
3	100	1400	0.04
4	120	1000	0.03
5	120	1200	0.04
6	120	1400	0.02
7	140	1000	0.04
8	140	1200	0.02
9	140	1400	0.03

The experiment was repeated three times to reduce the experimental error

Table 3. Observations for different output parameters of DMLS

Exp. No.	HV	Ra, μm	Δd, mm	SN for HV	SN for Ra	SN for Δd
1.	339.6±1.5	5.79±0.09	0.05±0.004	47.8855	− 15.2536	27.9588
2.	247.9±1.5	3.19±0.08	0.04±0.003	47.0591	− 10.0758	30.4576
3.	225.4±2.5	2.13±0.10	0.03±0.004	49.0847	− 6.5676	24.4370
4.	284.6±1.5	4.39±0.09	0.06±0.004	47.3023	− 12.8493	26.0206
5.	231.8±2.0	2.32±0.09	0.05±0.002	50.2457	− 7.3098	27.9588
6.	325.3±2.0	4.9±0.11	0.04±0.003	48.9988	− 13.8039	23.0980
7.	281.8±1.5	4.26±0.12	0.07±0.004	50.9801	− 12.5882	21.9382
8.	354±1.5	6.77±0.19	0.08±0.005	48.5107	− 16.6118	24.4370
9.	266.4±1.5	4.19±0.09	0.06±0.004	47.8855	− 12.4443	27.9588

(a) (b) (c)
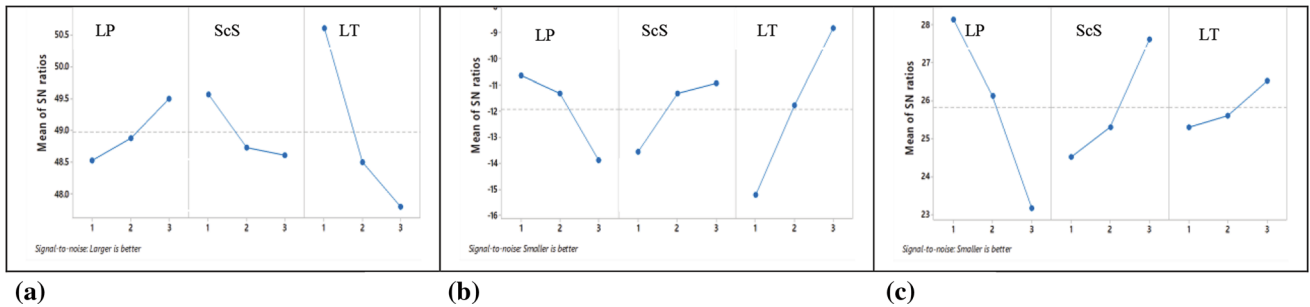
Fig. 11. Main effect plots for HV (a), Ra (b), and Δd (c)

Table 4. ANOVA for HV, Ra, and Δd

Source	DoF	Seq.SoS	Adj. MoS	F	P	%C
ANOVA for HV						
A	2	1.4610	0.73052	13.63	0.068	9.0
B	2	1.6542	0.82709	15.43	0.061	10.19
C	2	12.9994	6.49970	121.23	0.008	80.13
Residual error	2	0.1072	0.05362	…	…	0.66
Total	8	16.2219	…	…	…	…
ANOVA for Ra						
A	2	17.5866	8.7933	46.99	0.021	19.20
B	2	12.0246	6.0123	32.13	0.030	13.13
C	2	61.5721	30.7861	164.53	0.006	67.24
Residual error	2	0.3742	0.1871	…	…	0.40
Total	8	91.5576	…	…	…	…
ANOVA for Δd						
A	2	37.794	18.8968	30.02	0.032	66.25
B	2	15.570	7.7851	12.37	0.075	27.29
C	2	2.417	1.2083	1.92	0.342	4.33
Residual error	2	1.259	0.6294	…	…	2.20
Total	8	57.039	…	…	…	…

DoF: Degree of freedom, Seq. SoS: Sequential sum of squares, Adj. MoS: Adjusted mean of squares, F: Fisher's value, P: Probability, % C: Percentage contribution

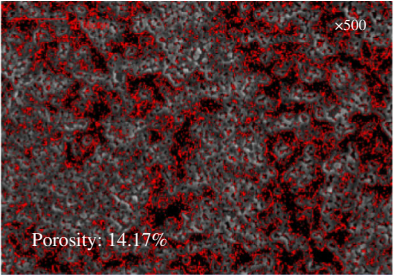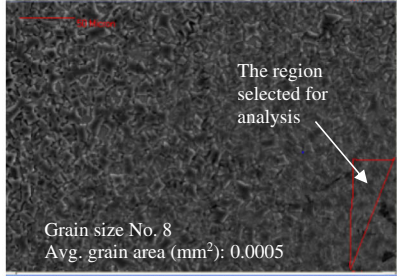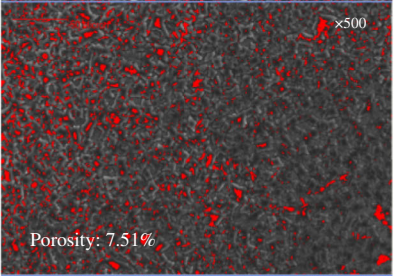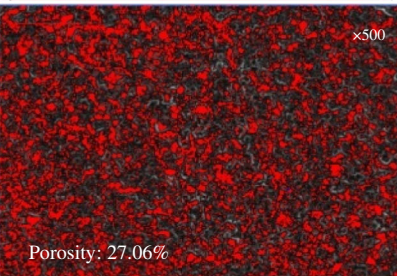**Table 5. Grain size number/area and porosity analysis**
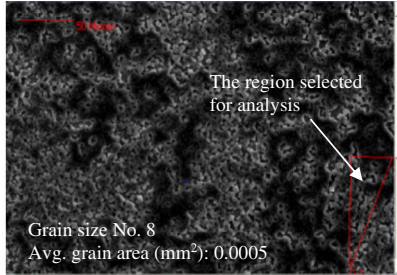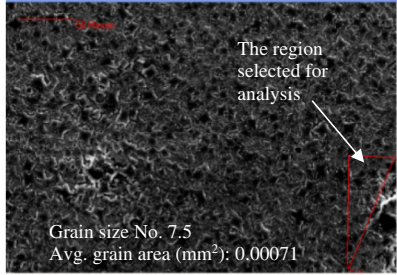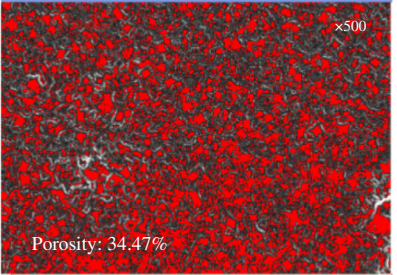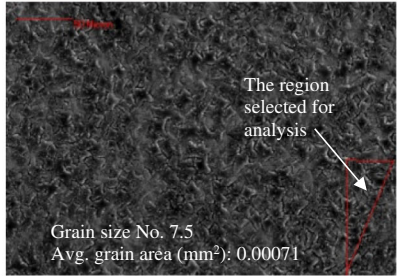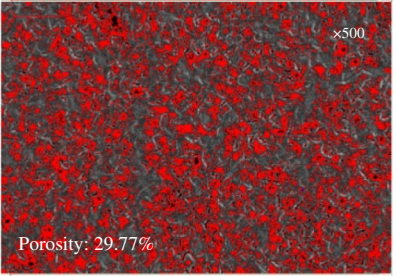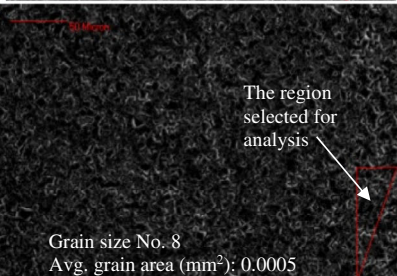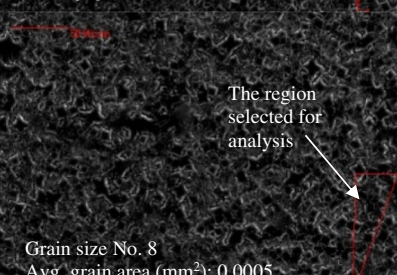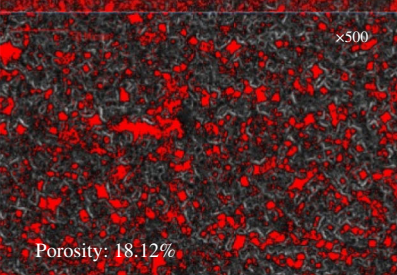
S.No.	Grain size number as per ASTM E 112	Porosity (%) as per ASTM B276
1.	The region selected for analysis. Grain size No. 8, Avg. grain area (mm²): 0.0005	×500, Porosity: 14.17%
2.	The region selected for analysis. Grain size No. 8, Avg. grain area (mm²): 0.0005	×500, Porosity: 7.51%
3.	The region selected for analysis. Grain size No. 7.5, Avg. grain area (mm²): 0,00071	×500, Porosity: 34.47%
4.	The region selected for analysis. Grain size No. 7.5, Avg. grain area (mm²): 0.00071	×500, Porosity: 29.77%
5.	The region selected for analysis. Grain size No. 8, Avg. grain area (mm²): 0.0005	×500, Porosity: 27.06%
6.	The region selected for analysis. Grain size No. 8, Avg. grain area (mm²): 0.0005	×500, Porosity: 18.12%

Table 5. continued

7. Grain size No. 8
Avg. grain area (mm²): 0.0005 — Porosity: 24.91% (×500)

8. Grain size No. 7.5
Avg. grain area (mm²): 0.00071 — Porosity: 25.55% (×500)

9. Grain size No. 8
Avg. grain area (mm²): 0.0005 — Porosity: 21.53% (×500)
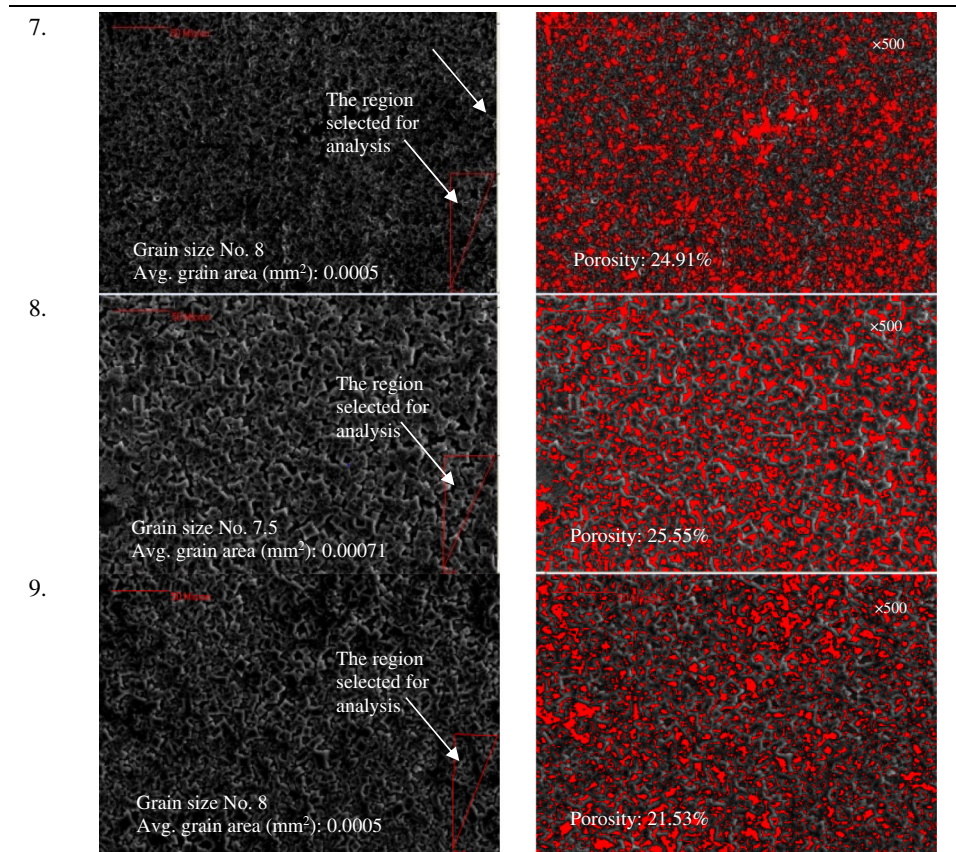
where η is SN ratio, n is the no. of experiment, and y is the material property at experiment no. k. Based upon SN ratio calculations, Fig. 11 shows main effect plots for HV, Ra, and Δd. The analysis of variance (ANOVA) was also performed using SN analysis for HV, Ra, and Δd (Table 4).

As observed from Fig. 11, for HV the best settings are: LP 140W, ScS 1000mm/s and LT 0.02mm. These settings are but obvious because the highest LP, minimum ScS, and minimum LT will provide more heat input to the functional prototype. The ANOVA analysis further clarified that %C for LT was highest, and this was the only significant factor (at 95% confidence level). For Ra and Δd, the LP 100W, ScS1400mm/s, and LT 0.4mm are observed as best settings. In the case of Ra, all three input parameters were observed as significant in ANOVA analysis (at 95% confidence level) with the highest %C of LT just similar to HV. Further, for Δd the highest %C was observed for LP, and this was observed as the only significant factor (at 95% confidence level).

Further based upon Table 2 and 5 show the grain size number, average grain area (as per ASTM E 112), and porosity (%) (as per ASTM B 276). As observed from Table 3, more hardness was observed in experiments no. 1, 6, and 8. It should

Table 6. 3D rendered images, ADF and PC analysis

Exp. No.	SEM images	3D rendered SEM image	ADF	PC
1.				
2.				
3.				
4.				
5.				
6.				

Table 6. continued
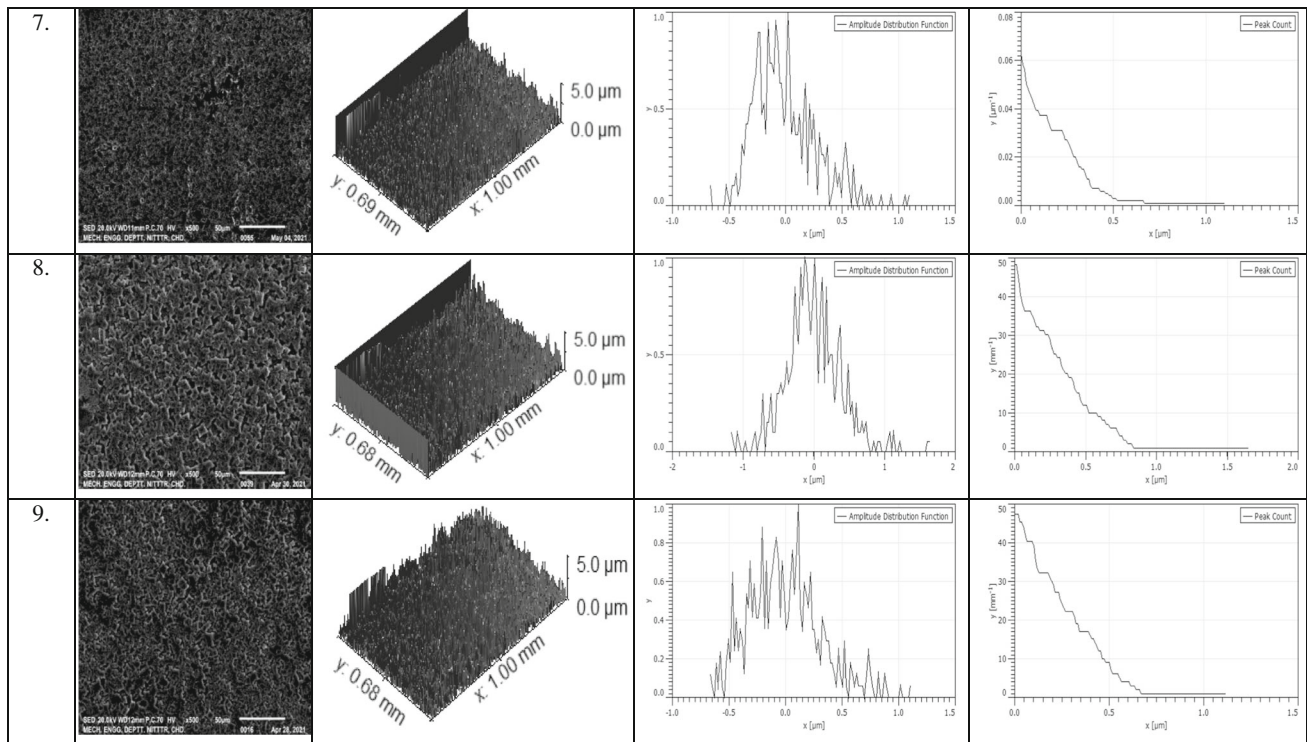
be noted that for these experimental settings, the LT was the same (0.02 mm), which was observed as the only significant parameter for HV (as per Table 4). Based upon grain size analysis, it has been noticed that for experiment no. 8, avg. grain area has increased, hence no. of grains per unit area is decreased. This may have contributed to higher HV, Ra, and Δd (Table 5). For further analysis, the SEM images were processed with open-source image processing software, and 3D rendered images of microstructure, amplitude distribution function (ADF) and peak count (PC) of Ra profile were calculated (Table 6). As observed from Table 6 for the sample prepared in experiment no. 8, the signature for ADF is more uniform (bell-shaped) as compared to experiment no. 1 and 6. Correspondingly the PC value for experiment no. 8 was also higher, which may have contributed to higher Ra and Δd.

Further for multifactor optimization, SN for Δd, Ra, and HV (observed in Table 3) was analyzed by assigning equal importance to HV (Table 7), and correspondingly, composite desirability was calculated. Based upon Table 7, Fig. 12 shows the optimization plot for Δd, Ra, and HV with optimized settings as 1–2–3 means LP 100W, ScS 1200 mm/s, and LT 0.02 mm.

Table 7. Response optimization: SN for Δd, SN for Ra, SN for HV (based upon Table 3)

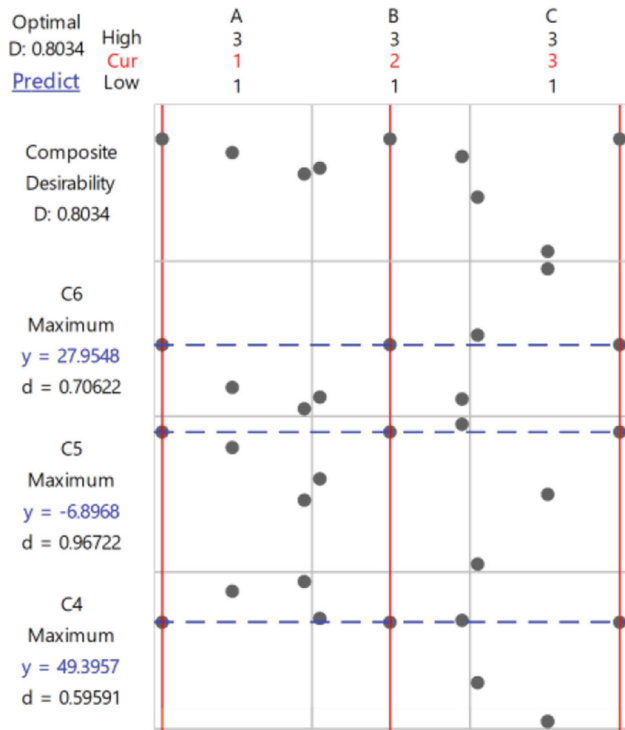| Response				Weight	Importance
SN for Δd				1	2
SN for Ra				1	3
SN for HV				1	1
Solution:					Composite
	A	B	C		Desirability
	1	2	3		0.8034

Fig. 12. Optimization plot for Δd, Ra, and HV

5. Conclusions

Following are the conclusions from this study:-

- The innovative IM pin profile on 17-4PH SS has been successfully prepared on DMLS setup after ascertaining the best profile (based upon veterinary surgical practices).
- The selected output parameters of DMLS were HV, Ra, and Δd. The results of the study suggest that for HV, LT is the only significant parameter with %C of 80.13%. For Ra of IM pins all three selected input parameters (LP, ScS, and LT) were significant. However, LT was observed as the most significant parameter with %C 67.24%. As regard to Δd, the most significant parameter was observed as LP with %C of 66.25%. These results are in line with morphological observations captured through SEM (based photomicrographs, 3D rendered images, porosity (%), and grain size number).
- From multifactor optimization view point best settings of DMLS are 100 W LP, 1200 mm/s ScS and 0.04 mm LT.
- The proposed IM pins are ready to use implants for ca-

nine with possible better retention capabilities leading to less invasive surgical practices.
- Further studies may be performed with different pin profiles, hollow sections, metamaterial-based 3D printing of IM pins for reducing the weight component and increasing the damping capabilities of the implant.

References

1. Standard, A.S.T.M., 2012. F2792-12a" Terminology for Additive Manufacturing Technologies". ASTM International. West Conshohocken https://doi.org/10.1520/F2792-12A
2. J.P. Kruth, M.C. Leu and T. Nakagawa, Progress in Additive Manufacturing and Rapid Prototyping, *CIRP Ann.*, 1998, **47**(2), p 525–540
3. D.T. Pham and S.S. Dimov, Rapid Prototyping and Rapid Tooling—The Key Enablers for Rapid Manufacturing, *Proc. Inst. Mech. Eng. C J. Mech. Eng. Sci.*, 2003, **217**(1), p 1–23
4. I. Campbell, O. Diegel, J. Kowen and T. Wohlers, *Wohlers Report 2018: 3D Printing and Additive Manufacturing State of the Industry: Annual Worldwide Progress Report*, Wohlers Associates, New York, 2018
5. L. Kumar, Q. Tanveer, V. Kumar, M. Javaid and A. Haleem, Developing Low-Cost 3 D Printer, *Int. J. Appl. Sci. Eng. Res.*, 2016, **5**(6), p 433–447
6. S. Peel, D. Eggbeer, H. Burton, H. Hanson and P.L. Evans, Additively Manufactured Versus Conventionally Pressed Cranioplasty Implants: An Accuracy Comparison, *Proc. Inst. Mech. Eng. [H]*, 2018, **232**(9), p 949–961
7. R. Bibb, D. Eggbeer, P. Evans, A. Bocca and A. Sugar, Rapid Manufacture of Custom-Fitting Surgical Guides, *Rapid Prototyp. J.*, 2009, **15**, p 346–354
8. A.J. Festas, A. Ramos and J.P. Davim, Medical Devices Biomaterials–A Review, *Proc. Inst. Mech. Eng. Part L J. Mater. Des. Appl.*, 2020, **234**(1), p 218–228
9. D.F. Williams, Biofunctionality and biocompatibility. *Materials Science and Technology*, 2006
10. M. Saini, Y. Singh, P. Arora, V. Arora and K. Jain, Implant Biomaterials: A Comprehensive Review, *World J. Clin. Cases*, 2015, **3**(1), p 52–57. https://doi.org/10.12998/wjcc.v3.i1.52
11. S. Hosseini, S. Mirdamadi and A. Nemati, Porous Ti6Al4V Scaffolds for Dental Implants: Microstructure, Mechanical, and Corrosion Behavior, *Proc. Inst. Mech. Eng. Part L J. Mater. Des. Appl.*, 2016, **230**(5), p 927–933
12. D.H. Kohn, P. Ducheyne, Materials for Bone and Joint Replacement. *Materials Science and Technology*, 2006
13. R.N. Brown, B.E. Sexton, T.M.G. Chu, T.R. Katona, K.T. Stewart, H.M. Kyung and S.S.Y. Liu, Comparison of Stainless Steel and Titanium Alloy Orthodontic Mini Screw Implants: A Mechanical and Histologic Analysis, *Am. J. Orthod. Dentofac. Orthop.*, 2014, **145**(4), p 496–504
14. I. Mutlu and E. Oktay, Biocompatibility of 17–4 PH Stainless Steel Foam for Implant Applications, *Bio-Med. Mater. Eng.*, 2011, **21**(4), p 223–233
15. L.E.E. Jae-Ho, J.A.N.G. Jeong-Hwan, J.O.O. Byeong-Don, Y.I.M. Hong-Sup and M.O.O.N. Young-Hoon, Application of Direct Laser Metal Tooling for AISI H13 Tool Steel, *Trans. Nonferrous Met. Soc. China*, 2009, **19**, p s284–s287
16. T. Duda and L.V. Raghavan, 3D Metal Printing Technology, *IFAC-PapersOnLine*, 2016, **49**(29), p 103–110

17. T. Altan, B. Lilly and Y.C. Yen, Manufacturing of Dies and Molds, *CIRP Ann.*, 2001, **50**(2), p 404–422

18. M. Krishnan, E. Atzeni, R. Canali, F. Calignano, D. Manfredi, E.P. Ambrosio and L. Iuliano, On the Effect of Process Parameters on Properties of AlSi10Mg Parts Produced by DMLS, *Rapid Prototyp. J.*, 2014, **20**, p 449–458

19. J. Delgado, J. Ciurana and C.A. Rodriguez, Influence of Process Parameters on Part Quality and Mechanical Properties for DMLS and SLM with Iron-Based Materials, *Int. J. Adv. Manuf. Technol.*, 2012, **60**(5–8), p 601–610

20. R.D.N. Libardoni, G.M.C. Serafini, C.D. Oliveira, P.I. Schimites, R.O. Chaves, J.P.S. Feranti, C.A.S. Costa, A.S.D. Amaral, A.G. Raiser and A.V. Soares, Appendicular Fractures of Traumatic Etiology in Dogs: 955 Cases (2004–2013), *Ciência Rural*, 2016, **46**(3), p 542–546

21. N. Rosa, M. Marta, M. Vaz, S.M. Tavares, R. Simoes, F.D. Magalhães and A.T. Marques, Intramedullary Nailing Biomechanics: Evolution and Challenges, *Proc. Inst. Mech. Eng. [H]*, 2019, **233**(3), p 295–308

22. P. Kumar and T.K. Gahlot, Clinical Evaluation of Intramedullary Pinning and Interlocking Nailing Technique for Stabilization of Femoral Fractures in Dogs, *J. Anim. Sci. Adv.*, 2013, **3**(6), p 310–313

23. C.P. Laurent, B. Böhme, J. Verwaerde, L. Papeleux, J.P. Ponthot and M. Balligand, Effect of Orthopedic Implants on Canine Long Bone Compression Stiffness: A Combined Experimental and Computational Approach, *Proc. Inst. Mech. Eng. [H]*, 2020, **234**(3), p 255–264

24. T.D. Braden and W.O. Brinker, Radiologic and Gross Anatomic Evaluation of Bone Healing in the Dog, *J. Am. Vet. Med. Assoc.*, 1976, **169**(12), p 1318–1323

25. M. Jagodzinski and C. Krettek, Effect of Mechanical Stability on Fracture Healing—An Update, *Injury*, 2007, **38**(1), p S3–S10

26. C.E. DeCamp, S.A. Johnston, L.M. Déjardin, S.L. Schaefer, The hip joint. *Brinker, Piermattei, and Flo's Handbook of Small Animal Orthopedics and Fracture Repair.* 5th and. St. Louis: Elsevier, 2016, pp. 468–517

27. P.C. Frake, R.J. Howell and A.S. Joshi, Strength of Titanium Intramedullary Implant Versus Miniplate Fixation of Mandibular Condyle Fractures, *Otolaryngol. Head Neck Surg.*, 2012, **147**(1), p 33–39

28. A. Kaur, A. Kumar, D. Kumar, J. Mohindroo and N.S. Saini, Feasibility of C-Arm Guided Closed Intramedullary Pinning for the Stabilization of Canine Long Bone Fractures, *Vet. World*, 2015, **8**(12), p 1410

29. K. Altunatmaz, S. Ozsoy, Z. Mutlu, Y. Devecioglu and O. Guzel, Use of Intramedullary Fully Threaded Pins in the Fixation of Feline and Canine Humeral, Femoral and Tibial Fractures, *Vet. Comp. Orthop. Traumatol.*, 2012, **25**(04), p 321–325

30. K.H. Kraus, S.M. Fox, F.S. Pike and E.C. Salzer, *Small Animal Fracture Repair: A Case-Based Approach*, CRC Press, London, 2016